Steel and Composite Structures, *Vol. 21, No. 3 (2016) 661-677*
DOI: http://dx.doi.org/10.12989/scs.2016.21.3.661

Seismic performances of steel reinforced concrete bridge piers

Jiangdong Deng [1a], Airong Liu [*2], Qicai Yu [1] and Guoxing Peng [1]

[1] *School of Civil Engineering, Guangzhou University, Guangzhou 510006, China*
[2] *Guangzhou University – Tamkang University Joint Research Center for Engineering Structure Disaster Prevention and Control, Guangzhou University, Guangzhou 510006, China*

(*Received September 25, 2015, Revised April 06, 2016, Accepted May 18, 2016*)

Abstract. The quasi static test of the steel reinforced concrete (SRC) bridge piers and rigid frame arch bridge structure with SRC piers was conducted in the laboratory, and the seismic performance of SRC piers was compared with that of reinforced concrete (RC) bridge piers. In the test, the failure process, the failure mechanism, hysteretic curves, skeleton curves, ductility coefficient, stiffness degradation curves and the energy dissipation curves were analyzed. According to the M-Φ relationship of fiber section, the three-wire type theoretical skeleton curve of the lateral force and the pier top displacement was proposed, and the theoretical skeleton curves are well consistent with the experimental curves. Based on the theoretical model, the effects of the concrete strength, axial compression ratio, slenderness ratio, reinforcement ratio, and the stiffness ratio of arch to pier on the skeleton curve were analyzed.

Keywords: steel reinforced concrete (SRC) pier; rigid frame arch bridge; reinforced concrete (RC) pier; seismic performances; skeleton curve

1. Introduction

Strong earthquakes frequently occur in the world. Bridge piers are easily damaged in earthquakes, which may lead to the bridge structural collapse. The steel reinforced concrete (SRC) pier is a new form of bridge pier with section steel inside and has good seismic mechanical performances. SRC pier has been increasingly applied in civil engineering, so the study on the seismic performance of SRC pier is important.

Azizinamini and Ghosh (1997) summarized typical damages of SRC structures in Japan during the Hyogoken- Nanbu Earthquake in 1995. A major factor of the collapse of many SRC buildings was the lack of adequate confining steel and cross ties, especially in large columns.

Hsu and Ghosh (2000) presented an experimental investigation of the inelastic behavior of SRC members under the periodically applied bending and torsional loads. Results indicated that the ultimate flexural capacity of an SRC member was significantly reduced under a moderate torsion degree.

Based on theoretical models, Liang *et al*. (2009) studied the constitutive bond-slip relation on the steel-concrete interface. The constitutive relation is relevant to the embedment length and the thickness of concrete cover.

*Corresponding author, Ph.D., E-mail: liu-a-r@163.com
[a] Ph.D., E-mail: dengjdong@qq.com

 ISSN: 1229-9367 (Print), 1598-6233 (Online)

Zhou and Liu (2010) investigated the seismic behavior of tubed SRC short columns. Three circular tubed SRC columns (CTSRC) and three square tubed SRC (STSRC) columns with two common SRC columns for comparison were tested under combined constant axial compression and lateral cyclic load. The lateral load strength of CTSRC and STSRC short columns increased with an increment in axial load level, while the axial load ratio has no obvious effect on the plastic deformation capacity. A modified ACI design method was adopted to calculate the nominal shear strength of STSRC columns as well as CTSRC columns.

Zhao *et al*. (2010) presented an experimental study of the behaviors of SRC composite columns and carried out nonlinear numerical analysis. The result showed that concrete strength had a significant effect on the load-carrying capacity of axially loaded columns, but had no significant effect on the eccentrically loaded columns.

Denavit *et al*. (2011) developed a three-dimensional distributed plasticity formulation for composite beam-columns suitable for nonlinear static and dynamic analyses of composite seismic force resisting systems. New uniaxial constitutive relations were developed for the concrete and steel elements to simulate the cyclic response of steel reinforced concrete (SRC) members.

Based on the principle of minimum potential energy, the interface slips in duplex steel reinforced concrete column was calculated by Liang *et al*. (2012), and a pull-out mechanics model of duplex steel reinforced concrete column had been established. The slip displacement on the interface of steel and concrete of the column along the embedment length was derived by the principle of minimum potential energy. The calculation results showed that the slip curves have the basic characteristics of quadratic curves distribute.

Based on the related theoretical analysis and experimental research, the method for calculating ultimate energy dissipation capacity of SRC column was proposed and the damage sensitivity were analyzed by Zheng *et al*. (2012). The research showed that sectional dimension was the most sensitive factor in the damage of SRC column and the steel ratio takes the second place, and then the strength of concrete was the most insensitive design parameter.

Chen *et al*. (2013) analyzed the mechanical properties of the remaining carrying capacity of steel reinforced concrete columns after exposure to fire. The temperature distribution law of the column cross-section in the case of uneven fire was obtained.

Ma *et al*. (2013) studied the seismic performance of steel-reinforced recycled concrete (SRRC) columns based on low cyclic loading tests of seven column specimens. The results indicated that the SRRC columns had good performance in terms of earthquake resistance.

Chen *et al*. (2015) found the failure modes for planar loading and spatial loading observed in the tests showed that the shear-diagonal compressive failure was the dominating failure mode for all the SRC specimens.

Wang *et al*. (2016) pointed out that the encased steel shape worked with the concrete compatibly due to the confinement from the steel tube, and the flange shear studs were not effective in enhancing the flexural stiffness and the axial resistance.

As for the skeleton curve theoretic model of SRC pier, Guo *et al*. (2009) conducted cyclic loading tests on 6 half-scaled SRC columns to investigate the effects of axial compression ratio and stirrup configuration on the seismic performance and hysteretic characteristics to give the theoretical model of the skeleton curve. Li and Tao (2013) collected 84-group test data of SRC columns from cyclic loading experiments for linear fitting, discussed the relationship between deformation, the bearing capacity and the concrete strength, axial compression ratio, stirrup characteristic value, and proposed the calculation method for the characteristic points of SRC column skeleton curve.

At present, the study on the seismic performances of steel reinforced concrete bridge piers is still rare, and the generally accepted conclusion has not yet established. In the paper, we conducted the quasi static tests of SRC piers and rigid frame arch bridge structure with SRC piers, analyzed the stress process under low cyclic loading, the failure pattern and mechanism, hysteretic curves, skeleton curves, ductility, stiffness degradation and energy dissipation capacity curves of the SRC piers, and compared the seismic performance with that of the reinforced concrete (RC) pier. Combined with the model test, the calculation model of the skeleton curve of SRC piers and rigid frame arch bridge structure were established according to the M-Φ relationship, and the key parameters of the skeleton curve were discussed. The theoretical model is more accurate and easy for application. The conclusions are important reference for theoretical analysis and engineering practice of steel reinforced concrete bridge piers.

2. Experimental program

2.1 Details of testing piers and materials

The details of bridge piers are shown in Table 1. The specimens were constructed with C40 concrete. The concrete consists of Portland cement, water, locally available sand and crushed granite rock with a weight ratio of 1.0:0.45:2.4:3.1. The cylinder compressive strength and elastic modulus of concrete are 28 MPa and 30.0 GPa, respectively. The cross section of piers is square with the size of 300 mm × 300 mm. RC bridge pier was configured with 6 Φ 25 steel bars, and SRC bridge piers were configured with 4 Φ 18 steel bars and 14# I-beam steel. The longitudinal reinforcement ratio of each specimen was close to 3.4%. The diameter and spacing of stirrups are 10 mm and 100 mm, respectively. The reinforcement drawings of the specimens are shown in Figs. 1, and mechanical indicators of steel are shown in Table 2.

The height of bridge pier is 1.5 m, and the distance between the two piers of rigid frame arch bridge structure is 3.4 m. The piers in rigid frame arch bridge structure are the same as the specimen of the SRC pier; the arch rib is steel pipe of 160 mm × 6 mm (diameter × thickness), and the arch rib connects with the piers at the corbel, as shown in Figs. 2 and 3. The rise-span ratio of rigid frame arch bridge structure is 1/5. Piers are fixed on the base. The base size of the piers is 1000 mm × 500 mm × 400 mm and the base size of rigid frame arch bridge structure is 4100 mm × 500 mm × 400 mm.

Table 1 Details of bridge piers

Pier No.	Structure forms	Axial compression ratio	Cross section of piers	Main reinforcement of piers	Stirrup of piers
RC-0.15	Reinforced concrete	0.15	Square	6Φ25	Φ10@100
SRC-0.15	Steel reinforced concrete	0.15	Square	4Φ18+14# steel I-beam	Φ10@100
SRC-0.2	Steel reinforced concrete	0.2	Square	4Φ18+14# steel I-beam	Φ10@100
SRC-STR	Rigid frame arch bridge structure with steel reinforced concrete piers	0.15	Square	4Φ18+14# steel I-beam	Φ10@100

Table 2 Mechanical properties of steel

Steel shape	Steel type	Elastic modulus (Gpa)	Test yield strength (Mpa)	Test tensile strength (Mpa)
Φ25	HRB335	200	345	525
Φ18	HRB335	200	390	580
Φ10	HPB235	210	360	540
I-beam steel	HRB235	210	320	435

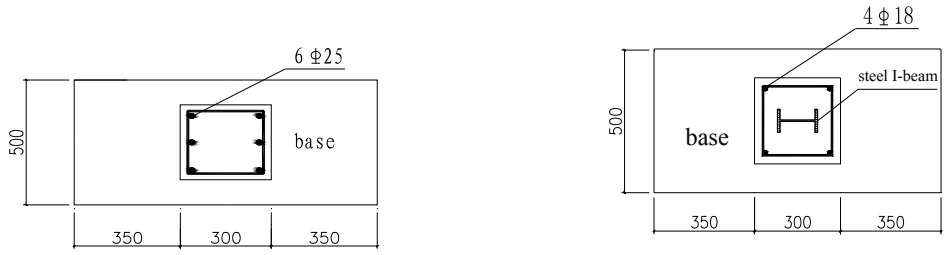

(a) RC bridge pier (b) SRC bridge pier

Fig. 1 Section drawing

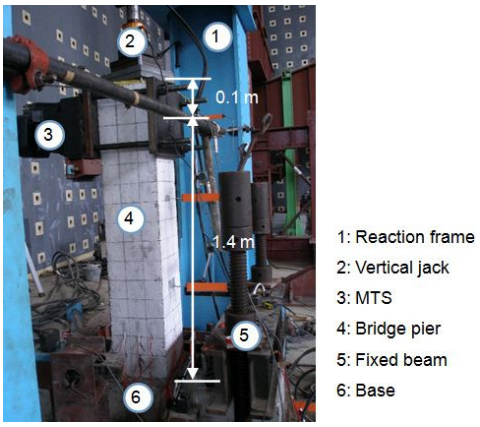

Fig. 2 RC or SRC bridge pier

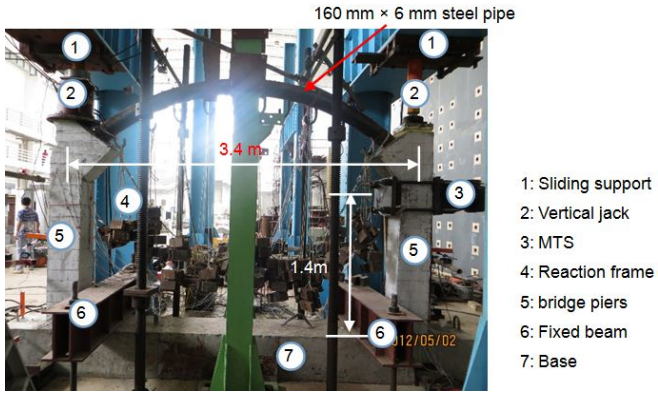

Fig. 3 Rigid frame arch bridge structure with SRC piers

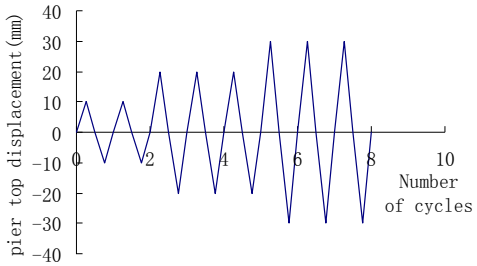

Fig. 4 Loading rules

2.2 Loading equipment

MTS is used as loading equipment to generate the cyclic horizontal load. The vertical hydraulic jack provides the constant axial force. The vertical hydraulic jack is placed under the sliding support which is connected with the reaction frame. The base of the specimen is fixed with the fixed beam. The loading height of piers is 1.4 m. The data of horizontal and vertical loads are collected and recorded by computer. The device used in this experiment is shown in Figs. 2 and 3.

2.3 Loading regimes

In this test, the force-displacement controlled loading method was used. The loading rules were shown in Fig. 4. At first the horizontal loading was implemented through the force-controlled method and each load was repeated for 2 times. After the yield force, the displacement-controlled loading method was used, and each displacement was repeated for 3 times. When the horizontal load was less than 0.85 times of the maximum load value, the specimen was regarded as failure, and the test was terminated.

3. Testing results

3.1 Failure mode

In the initial force-controlled loading phase, all the piers kept in the elastic state, showing the good seismic mechanical performances. In the later displacement-controlled loading phase, the failure modes of piers showed the significant difference.

As for the RC pier, during the later loading process, the horizontal and inclined cracks appeared at the pier bottom. Then inclined cracks were extended, crossed, and linked with each other. At last along with the development of cracks, a large quantity of concrete fell off and the piers failed. It showed significant flexural-shear failure characteristics. Fig. 5(a) is the failure photo of the RC bridge pier (RC-0.15).

The SRC piers with the axial compression ratios of 0.15 and 0.2 showed the similar failure mode. When the displacement of pier top was small, many horizontal cracks were initiated, and inclined crack development was not significant. When the displacement of pier top was large, the horizontal cracks rapidly developed, and a few inclined cracks formed, but inclined cracks were not connected with each other. Finally, concrete at pier bottom fell off; longitudinal steel bars were broken, and the SRC pier failed. The piers showed significant flexural failure characteristics. Fig. 5(b) is the failure photo of the SRC bridge pier with axial compression ratio of 0.15 (SRC-0.15).

Fig. 5(c) is the failure photo of the SRC pier of rigid frame arch bridge structure (STR-SRC). In the initial loading stage, concrete cracks within the height of 10~20 cm at pier bottom began to appear and increase. In the later loading stage concrete cracks penetrated pier bottom and concrete fell off. The bearing capacity of the structure declined. After the load was removed, cracks were not closed, and the pier top displacement could not be restored, so the test was terminated. The STR-SRC pier showed flexural failure characteristics.

3.2 Hysteretic curve

Figs. 6(a)-(d) show the hysteretic curves of pier bottom shear force - pier top lateral displacement.

(a) RC-0.15

(b) SRC-0.15

(c) SRC-STR

Fig. 5 Failure photos of the piers

As shown in Fig. 6(a), the hysteretic loop of RC pier is arched, and hysteretic curve shape is plump, indicating that the plastic deformation performance and energy absorption capacity of the RC pier is good. In Figs. 6(b) and Fig. (c), the hysteretic loop of SRC piers is fusiform, and hysteretic curve shape is plumper than that of RC pier, indicating that the plastic deformation capacity of the SRC pier is better and the pier can better absorb the earthquake energy.

In Fig. 6(d), the unloading segment of SRC-STR pier is straighter than that of the SRC piers, and the plastic deformation of SRC-STR reduces. In the later loading stage the hysteretic loops of SRC-STR do not coincide with each other under the same lateral displacement.

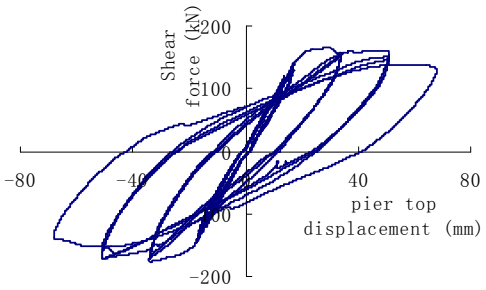

(a) The hysteretic curve of RC-0.15 pier

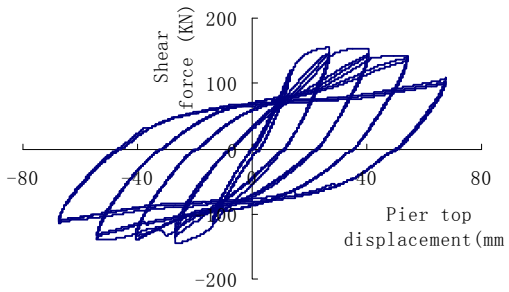

(b) The hysteretic curve of SRC-0.15 pier

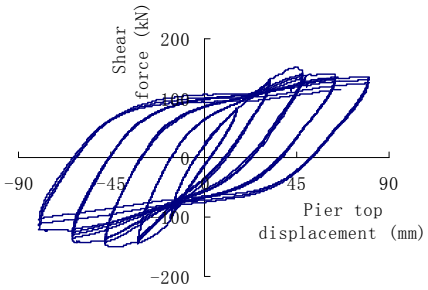

(c) The hysteretic curve of SRC-0.2 pier

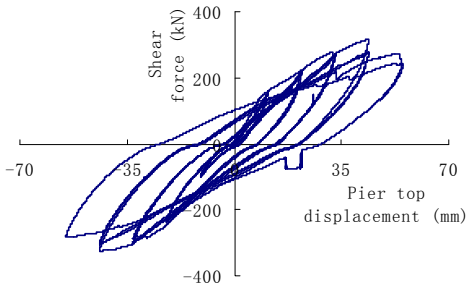

(d) The hysteretic curve of SRC-STR pier

Fig. 6 Hysteretic curves of pier bottom shear force- pier top lateral displacement

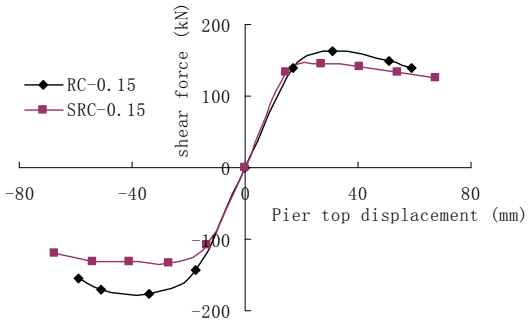

(a) Comparison of RC bridge piers and SRC pier

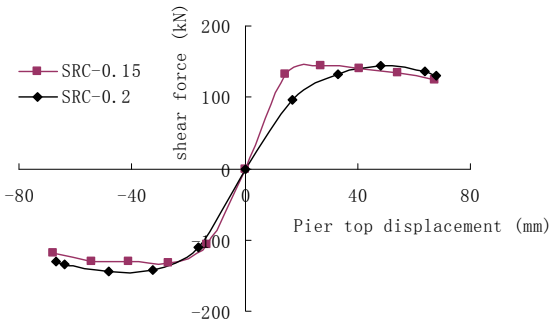

(b) Comparison of axial compression ratios

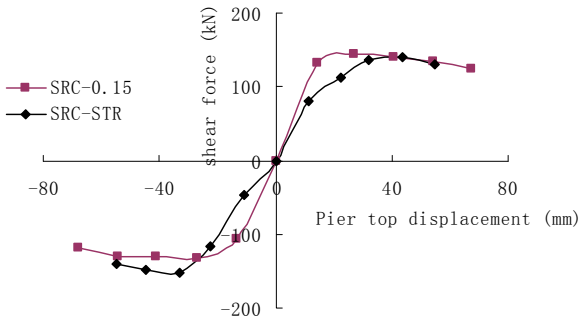

(c) Comparison of SRC bridge pier and rigid frame arch bridge structure

Fig. 7 Comparison of skeleton curves

3.3 Skeleton curve

The comparison of the skeleton curves is shown in Fig. 7. Because the rigid frame arch bridge structure has two piers, half of the lateral force is selected to compare with that of the SRC pier.

As shown in Fig. 7, the ultimate strength of RC-0.15 pier is 22% larger than that of SRC-0.15 pier because the steel bars in the RC pier are further from the neutral axis than the steel I-beam in SRC pier and the steel bars of RC beam can provide more contribution to the ultimate strength. But the ultimate displacement of RC-0.15 pier is 13% smaller than that of SRC-0.15 pier. The ultimate strength of the SRC-0.15 pier is smaller than that of the SRC-0.2 pier, and the ultimate displacement of SRC-0.15 is close to that of SRC-0.2.

Because of the influence of arch rib, a reverse moment occurs on the pier top of rigid frame arch bridge (Fig. 16). The reverse moment reduces the moment at pier bottom and generates a reverse deformation. Then the positive and negative average of ultimate strength of the rigid frame arch bridge structure is 6% higher than that of the SRC-0.15 pier, and the ultimate displacement of the rigid frame arch bridge structure is 80.6% of that of the SRC-0.15 pier.

The speed to the peak load of small axial compression pier (SRC-0.15) is faster than that of the large axial compression pier (SRC-0.2). Because the arch rib shares the load, the speed to the peak load of rigid frame arch bridge structure (SRC-STR) is significantly slower than that of the bridge pier specimens (SRC-0.15).

The descent stage of the load degradation curve indicates the beginning of the structure resistance degradation and stiffness degradation. If this parameter degrades quickly, the specimen will be destroyed easily. The load degradation speed of rigid frame arch bridge structure (SRC-STR) is the fastest, followed by RC-0.15 and SRC-0.15.

3.4 Ductile

Ductility can reveal the elastic-plastic deformation capacity of a structure or a member. The ductility coefficient μ is defined as

$$\mu = \Delta_{\max} / \Delta_y \tag{1}$$

where, $\Delta_{\max}$ is the failure displacement (ultimate displacement); Δ_y is the yield displacement, which can be obtained by the strain of the steel bar in the test.

Table 3 gives the pier displacement data and ductility coefficient value.

As can be seen from Table 3, the ductility coefficients of the pier are more than 3.0, indicating that the piers all exhibit high ductility capacity. The ductility capacity of the piers decreases in the following sequence: SRC bridge piers, rigid frame arch bridge structure, and RC bridge pier.

Table 3 Measured displacement and ductility coefficient

Specimens	Yield displacement (mm)	Failure displacement (mm)	Ductility coefficient
RC-0.15	17.1	59.1	3.5
SRC-0.15	16.0	67.7	4.2
SRC-0.2	15.1	64.0	4.2
SRC-STR	14.6	54.0	3.7

3.5 Stiffness degradation curve

Stiffness degradation is an important indicator to reflect the seismic behavior of the piers. The stiffness can be indicated as the secant stiffness

$$K_i = \frac{|+F_i|+|-F_i|}{|+\Delta_i|+|-\Delta_i|} \tag{2}$$

where, $\pm F_i$ are the peak loads in the ith cycle; $\pm \Delta_i$ are the peak displacements in the ith cycle.

The stiffness degradation curves are shown in Fig. 8. The stiffness of RC pier is bigger than that of SRC pier. In the initial loading stage, the stiffness of SRC-0.15 is larger than the stiffness of SRC-0.2 and SRC-STR; and in the later loading stage, the stiffness of the three specimens is almost the same.

3.6 Energy dissipation analysis

The equivalent viscous damping coefficient h_e is commonly used to indicate hysteretic energy dissipation capacity, and h_e is defined as

$$h_e = \frac{1}{2\pi}\frac{S_{ABC}+S_{CDA}}{S_{OBE}+S_{ODF}} \tag{3}$$

where, $S_{ABC} + S_{CDA}$ is the energy dissipation of hysteretic loop; $S_{ABC} + S_{CDA}$ and $S_{OBE} + S_{ODF}$ can be calculated according to Fig. 9.

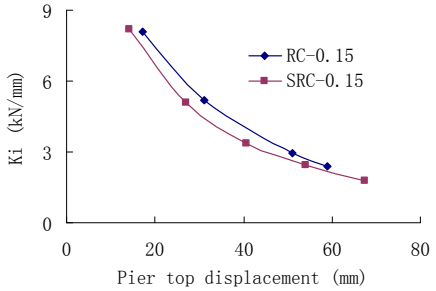

(a) Comparison of RC piers and SRC pier

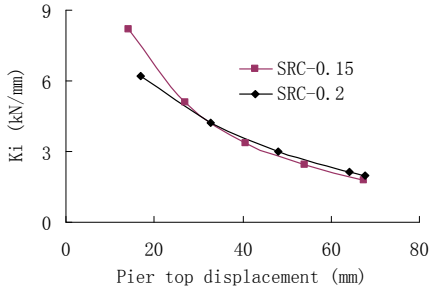

(b) Comparison of axial compression ratio

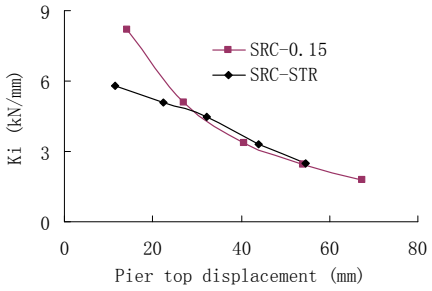

(c) Comparison of SRC bridge pier and rigid frame arch bridge structure

Fig. 8 Comparison of stiffness degradation curves

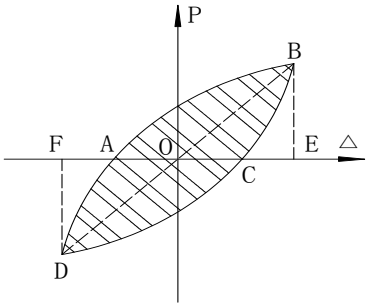

Fig. 9 Calculation of equivalent viscous damping coefficient

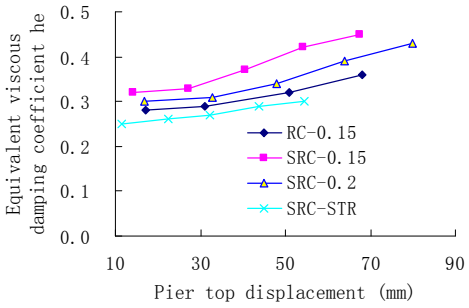

Fig. 10 Equivalent viscous damping coefficient

Fig. 10 shows the relationship of equivalent viscous damping coefficient and displacement of each specimen in the plastic state. It can be seen that as the displacement increases, the equivalent viscous damping coefficient increases. The equivalent viscous damping coefficient of various piers increases in the following sequence: SRC-STR, RC-0.15, SRC-0.2 and SRC-0.15, indicating that the SRC bridge piers have good energy dissipation capacity. The hysteretic loop of rigid frame arch bridge structure is not as plump as that of the bridge piers, so its equivalent viscous damping coefficient is small.

4. Calculation model of the skeleton curve

4.1 M-Φ curve of the section

4.1.1 Material constitutive model

Concrete is simulated with the Mander model, as shown in Fig. 11. The concrete is C40 and the ultimate strength of concrete is 28 MPa. Considering the constraint effect of the stirrups, the ultimate strength of concrete in the confinement area is (Guo and Shi 2003)

$$f_{c,c} = (1 + 2\lambda_c) f_c \tag{4}$$

where, λ_t is confinement index, $\lambda_t = \mu_t \dfrac{f_{yt}}{f_c}$; μ_t is the volumetric ratio of stirrups; f_c is the ultimate strength of concrete; f_{yt} is tensile strength of stirrups

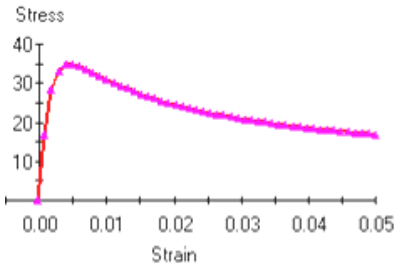

Fig. 11 Concrete Mander model (stress unit: MPa)

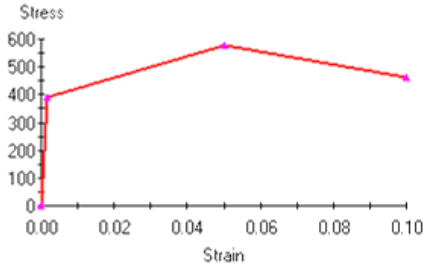

Fig. 12 Steel constitutive model (stress unit: MPa)

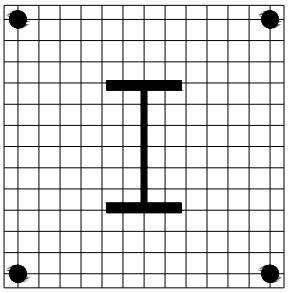

Fig. 13 Fiber cross-section of SRC pier

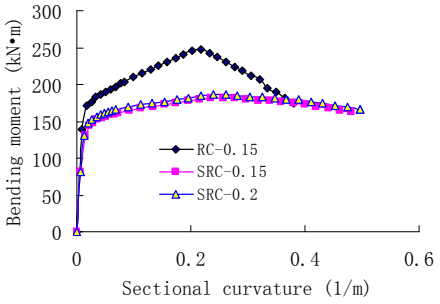

Fig. 14 M-Φ curves

Constitutive model of steel is shown in Fig. 12. At the beginning, the stress increases linearly to the yield stress, and then reaches the ultimate stress when the strain is 0.05. When the ultimate strain reaches 0.1 (Ministry of Transport of P.R.C. 2008), the corresponding stress is 0.8 times of the ultimate stress. The elastic modulus, steel yield strength and ultimate strength were the measured values shown in Table 2.

4.1.2 M-Φ curve calculation

In the calculation of M-Φ curve, fiber cross-section is used, as shown in Fig. 13. The size of concrete fiber is 22.5 mm, and the thickness of concrete cover is 15 mm.

The M-Φ curves are calculated by the section analysis software XTRACT, as shown in Fig. 14. It can be seen that the section bending moment of RC-0.15 is larger than that of SRC-0.15, and section bending moment of RC-0.15 declines more rapidly after the ultimate bending moment. The section ultimate curvature of RC-0.15 is 76.3% of that of SRC-0.15, indicating that the SRC pier has the good section deformation capacity. This is mainly because the section steel works at full capacity in late loading stage. The M-Φ curves of SRC-0.15 and SRC-0.2 are slightly different.

4.2 The skeleton curve of piers

The yield displacement of pier top can be calculated as follows

$$\Delta_y = \frac{1}{3}\phi_y H^2 \tag{5}$$

where, ϕ_y is the curvature of elastic-nonlinear turning point of M-Φ curve; H is the pier height.

The pier top displacement for the maximum load is

$$\Delta_m = \frac{1}{3}\phi_y H^2 + \frac{\phi_m - \phi_y}{2} L_p H \tag{6}$$

where, ϕ_m is the curvature for the maximum loading; L_p is the length of the plastic hinge. In Eurocode 8 L_p is (0.4~0.6) h, in which h is the height of the section. In this paper, L_p of the RC and SRC pier is selected as 0.5 h.

In the ultimate failure status, the pier top displacement is

$$\Delta_m = \frac{1}{3}\phi_y H^2 + \frac{\phi_m - \phi_y}{2} L_p H \tag{7}$$

where, ϕ_u is the curvature when the steel bar reaches the ultimate strain (0.1).

Without considering the second-order effect of gravity, the lateral force corresponding to a certain curvature on M-Φ curve can be expressed as

$$P = \frac{M}{H} \tag{8}$$

where, M is the bending moment corresponding to a certain curvature.

The comparison results of theoretical three wire skeleton curves and experimental curves are shown in Fig. 15. The theoretical curves basically coincide with experimental curves, indicating that the theoretical skeleton curves have the high precision.

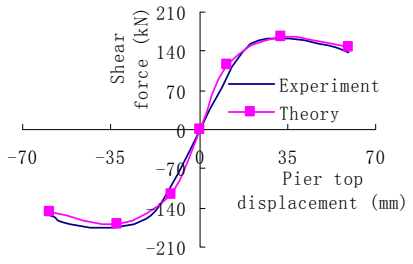

(a) RC-0.15 pier

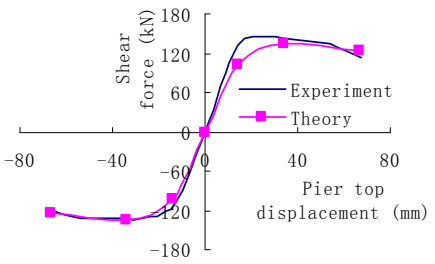

(b) SRC-0.15 pier

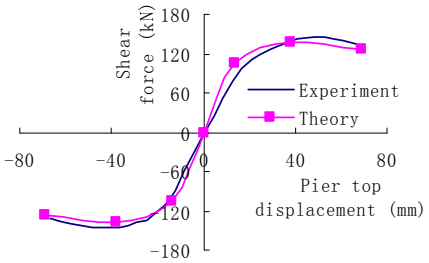

(c) SRC-0.2 pier

Fig. 15 Comparison of theoretical skeleton curves and experimental curves of the piers

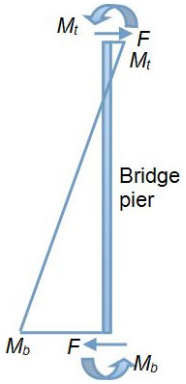

Fig. 16 Force analysis of rigid frame arch bridge piers

4.3 Skeleton curve of rigid frame arch bridge structure

The force analysis of the pier of rigid frame arch bridge structure is shown in Fig. 16. Pier top is subjected to a lateral force F ($F = 0.5P$, in which P is the lateral force applied on the rigid frame arch bridge structure) and a bending moment M_t.

The moment of pier top and bottom can be calculated according to the method of structural mechanics. In this test, the moment on pier top is $M_t = 0.06PH$, and the moment of pier bottom is calculated as $M_b = 0.44PH$.

Under the lateral force and moment, the arch bridge pier top displacement can be calculated as follows

$$\Delta_y = \frac{1}{3}\frac{5PH}{M_b}\phi_y H^2 + \frac{1}{2}\frac{M_t}{M_b}\phi_y H^2. \tag{9}$$

The pier top displacement for the maximum load in M-Φ curve is

$$\Delta_m = \frac{1}{3}\frac{0.5PH}{M_b}\phi_y H^2 - \frac{1}{2}\frac{M_t}{M_b}\phi_y H^2 + \frac{\phi_m - \phi_y}{2}L_p H. \tag{10}$$

The plastic hinge length of the piers in arch bridge structure is the same as the pier members, as shown in Eqn. (6).

When the ultimate failure state is achieved, the pier top displacement is

$$\Delta_u = \frac{1}{3}\frac{0.5PH}{M_b}\phi_y H^2 - \frac{1}{2}\frac{M_t}{M_b}\phi_y H^2 + \frac{\phi_u - \phi_y}{2}L_p H. \tag{11}$$

Without considering the second-order effect of gravity, the lateral force corresponding to a certain curvature of the pier in rigid frame arch bridge can be expressed as

$$P = \frac{M_b}{0.44H}. \tag{12}$$

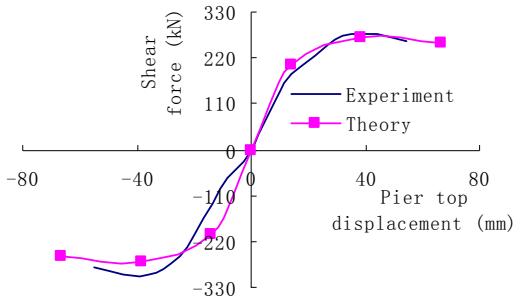

Fig. 17 Comparison of theoretical skeleton curve and experimental curve of SRC-STR

The comparison results of theoretical three-wire skeleton curve and experimental curve of the rigid frame arch bridge structure is shown in Fig. 17.

5. Influence parameters on the skeleton curve of SRC piers

The influence effect of different parameters on skeleton curve of SRC piers is analyzed according to the theoretical skeleton curve model. The reinforcement, the material performance, the loading height and the section size of SRC pier in analysis is the same as the model test. The axial compression ratio is 0.15.

5.1 Effect of concrete strength

The effect of concrete strength on the skeleton curve is shown in Fig. 18. With the increase of concrete strength, the ultimate force increases and the ultimate force is reached faster, and after reaching the ultimate force the descent line is steeper.

5.2 Effect of axial compression ratio

The effect of axial compression ratio on the skeleton curve is shown in Fig. 19. When axial compression ratio increases from 0.05 to 0.4, the ultimate load increases from 122.9 kN to 140.7 kN. The influence of axial compression ratio on the ultimate displacement is not obvious. The theoretical conclusion and experimental phenomenon is consistent.

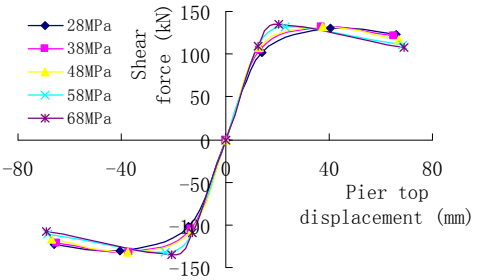

Fig. 18 Effect of concrete strength on the skeleton curve

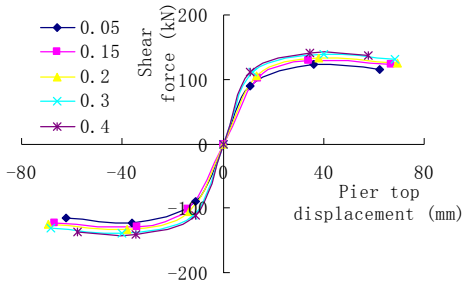

Fig. 19 Effect of axial compression ratio on the skeleton curve

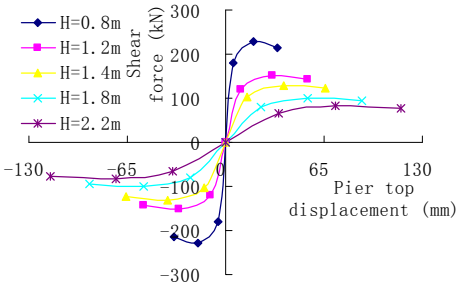

Fig. 20 Effect of slenderness ratio on the skeleton curve

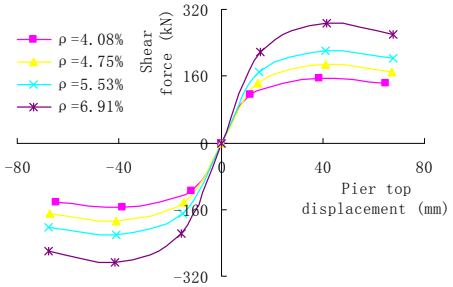

Fig. 21 Effect of reinforcement ratio on the skeleton curve

5.3 Effect of slenderness ratio

The effect of slenderness ratio on the skeleton curve is shown in Fig. 20. When pier height increases from 0.8 m to 2.2 m, the ultimate load reduces from 228 kN to 82.7 kN, and the ultimate deformation capacity increases from 34.1 mm to 116 mm. With the increase of the slenderness ratio, the descending segment of skeleton curve after the ultimate load becomes more flat.

5.4 Effect of reinforcement ratio

The effect of reinforcement ratio on the skeleton curve is obtained under the same 14# I-beam steel and different diameters of steel bars, as shown in Fig. 21. When the reinforcement rate ρ increases from 4.08% to 6.91%, the ultimate bearing capacity is significantly increased from 154.2 kN to 285.7 kN, and the ultimate displacement slightly increases from 64.8 mm to 67.9 mm.

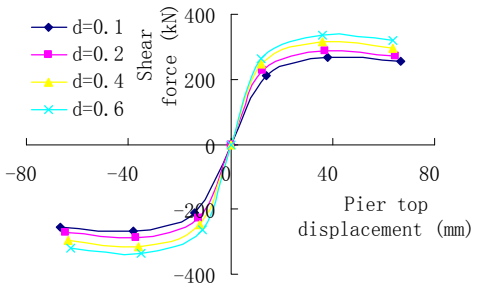

Fig. 22 Effect of arch-pier stiffness ratio on the skeleton curve

5.5 Stiffness ratio of arch rib to pier

The stiffness ratio of the arch rib to the pier is defined as $d = \frac{I_{arch}}{I_{pier}}$, and the effect of d on the skeleton curve is shown in Fig. 22. With the increase of d, the larger load is applied on arch rib, thus causing the increase of the ultimate load. When d is increased from 0.10 to 0.6, the ultimate load is increased from 268.6 kN to 337.7 kN and the ultimate displacement is decreased slightly from 66.8 mm to 63.5 mm.

6. Conclusions

In this paper, based on the model test and theoretic analysis the seismic performances of SRC piers were studied. The main findings of this study are summarized as follows:

(1) In the test, RC pier shows flexural-shear failure mode, and SRC pier shows flexural failure mode. Compared with the RC-0.15, SRC-0.15 pier shows the decreased ultimate load, the increased ultimate displacement, the lower stiffness, and the increased ductility and energy dissipation capacity.

(2) Compared with the SRC-0.15, SRC-0.2 shows the increased ultimate load and the decreased hysteretic energy dissipation capacity. The ultimate deformation, ductility performance, and stiffness in the latter loading stage of SRC-0.2 are close to those of SRC-0.15.

(3) Compared with the pier member of SRC-0.15, rigid frame arch bridge structure has straighter unloading segment in hysteretic curve, the increased ultimate bearing capacity, the decreased ultimate deformation, the decreased ductility, and the decreased energy dissipation capacity. The stiffness of the two specimens in the latter loading stage is similar.

(4) Based on M-Φ relationship, the three-wire theoretical model can be used to accurately calculate the force-displacement skeleton curve and simulate the nonlinear behaviors of bridge pier and rigid frame arch bridge structure.

(5) As for the SRC pier, according to the theoretical analysis, when concrete strength increases, the ultimate load increases and the descending segment after the ultimate load becomes steeper. With the increases of axial compression ratio and reinforcement ratio, the ultimate strength increases. When the slenderness ratio increases, the ultimate load quickly decreases; the ultimate deformation increases; and the descending segment after the ultimate load becomes more flat. With the increase of the stiffness ratio of arch to pier, the

bearing capacity of rigid frame arch bridge structure increases, and the ultimate displacement slightly decreases.

Acknowledgments

The project was financially supported by the National Natural Science Foundation of China (No. 51308137 and 51378133), Natural Science Foundation of Guangdong Province (No. 2014A030313530), Science and Technology Planning Project of Guangzhou City (No. 201607010094).

References

Azizinamini, A. and Ghosh, S.K. (1997), "Steel reinforced concrete structures in 1995 hyogoken-nanbu earthquake", *J. Struct. Eng.*, **12**(8), 986-992.

Chen, J.H., Ma, C., Li, J.H. and Qian, Q. (2013), "Temperature field analysis of steel reinforced concrete column in fire", *Appl. Mech. Mater.*, **351-352**, 615-618.

Chen, Z.P., Xu, J.J., Chen, Y.L. and Xue, J.Y. (2015), "Seismic behavior of steel reinforced concrete (SRC) t-shaped column-beam planar and 3d hybrid joints under cyclic loads", *Earthq. Struct., Int. J.*, **8**(3), 555-572.

Denavit, M.D., Hajjar, J.F. and Leon, R.T. (2011), "Seismic Behavior of Steel Reinforced Concrete Beam-Columns and Frames", *Structures Congress 2011 - Proceedings of the 2011 Structures Congress*, Las Vegas, NA, USA, April, pp. 2852-2861.

Guo, Z.H. and Shi, X.D. (2003), *Reinforced Concrete Theory and Analyse*, Tsinghua Uuniversity Press, Beijing, China. [In Chinese]

Guo, Z.X., Zhang, Z.W., Huang, Q.X. and Liu, Y. (2009), "Experimental study on hystereticmodel of SRC columns", *J. Earthq. Eng. Eng. Vib.*, **29**(5), 79-85.

Hsu, H.L. and Wang, C.L. (2000), "Flexural torsional behaviour of steel reinforced concrete members subjected to repeated loading", *Earthq. Eng. Struct. Dyn.*, **29**(5), 667-682.

Li, K.J. and Tao, Q.L. (2013), "Study on calculating method of skeleton curve characteristic-points of SRC column", *J. Anhui Univ. Technol.* (*Natural Science*), **30**(1), 71-77.

Liang, B., Meng, F.S. and Liu, J.L. (2009), "Research on bond-slip constitutive relation for steel reinforced concrete members", *J. Beijing Inst. Technol.* (*English Ed.*), **18**(2), 152-156.

Liang, B., Liu, X.M. and Mao, R. (2012), "Calculation of interface slips in duplex steel reinforced concrete column by principle of minimum potential energy", *Proceedings of the 12th International Symposium on Structural Engineering*, *ISSE*, Wuhan, China, November, pp. 824-827.

Ma, H., Xue, J.Y., Zhang, X.C. and Luo, D.M. (2013), "Seismic performance of steel-reinforced recycled concrete columns under low cyclic loads", *Construct. Build. Mater.*, **48**, 229-237.

Ministry of Transport of P.R.C. (2008), *Guidelines for Seismic Design of Highway Bridge* (*JTG/T B02-01-2008*), China Communications Press, Beijing, China. [In Chinese]

Wang, X.D., Liu, J.P. and Zhou, X.H. (2016), "Behaviour and design method of short square tubed-steel-reinforced-concrete columns under eccentric loading", *J. Construct. Steel Res.*, **116**, 193-203.

Zhao, G.T., Zhang, M.X. and Li, Y.H. (2010), "Strength and behaviour of slender steel reinforced concrete composite columns", *Adv. Struct. Eng.*, **13**(2), 231-239.

Zheng, S.S., Hu, Y., Tao, Q.L. and Li, Z.Q. (2012), "Damage sensitivity analysis for main design parameters of steel reinforced concrete column", *Adv. Mater. Res.*, **374-377**, 2566-2569.

Zhou, X.H. and Liu, J.P. (2010), "Seismic behavior and strength of tubed steel reinforced concrete (SRC) short columns", *J. Construct. Steel Res.*, **66**(7), 885-896.

CC